International Journal of Analytical, Experimental and Finite Element Analysis
Volume 10, Issue 4, December 2023, pp 134 - 150
https://doi.org/10.26706/ijaefea.4.10.20232000

Optimizing Crash Performance in Aluminum-Polyamide Hybrid Material Systems: Insights from Drop-Weight and Quasi-Static Indentation Testing

Ihab S. Hasan[1,*], Emad Q. Hussein[2]

College of Engineering, University of Kerbala, Karbala, Iraq.

[1]ihab.sh@s.uokerbala.edu.iq, [2]emad.dujaily@uokerbala.edu.iq

* Corresponding Author Email: ihab.sh@s.uokerbala.edu.iq

Abstract: This study delves into the behavior and performance of hybrid material systems, specifically focusing on the synergy between aluminum and polyamide-based composites during impact events. Through a series of quasi-static indentation and drop-weight impact tests, the research evaluates the dent resistance, energy absorption, and interface interactions of these materials. Results indicate that while composite laminates provide superior resistance to surface denting in low-energy impacts, aluminum exhibits vulnerability. However, when strategically combined, these materials offer mutual benefits, enhancing overall performance. Key findings reveal the significance of having a ductile material on the top surface to dissipate contact stresses and a sturdier bottom material to resist impact-induced bending. Furthermore, the threshold for delamination between the hybrid materials is identified, with indications that enhancing interfacial bond strength can elevate this threshold. This research underscores the importance of judicious hybrid material design for optimizing crash performance and sheds light on potential applications in automotive and aerospace industries, where both impact resistance and aesthetics are paramount.

Keywords: Hybrid material systems, Quasi-static indentation, Drop-weight impact, Aluminum-polyamide composites, Energy absorption, Interfacial bond strength, Dent resistance, Impact-induced bending, Material design, Crash performance.

Review – Peer Reviewed
Received: 26 October 2023
Accepted: 15 December 2023
Published: 30 December 2023

Cite this article: Ihab S. Hasan, Emad Q. Hussein, "Optimizing Crash Performance in Aluminum-Polyamide Hybrid Material Systems: Insights from Drop-Weight and Quasi-Static Indentation Testing", *International Journal of Analytical, Experimental and Finite Element Analysis*, RAME Publishers, vol. 10, issue 4, pp. 134-150, 2023. https://doi.org/10.26706/ijaefea.4.10.20232000

1. Introduction

Our preceding discussion established that spontaneous adhesion between distinct material sets is not just achievable but also modifiable through subtle alterations in processing parameters. With this foundational understanding, our focus shifts to discerning the significance of these adhesion variances on the mechanical attributes of a composite entity.

We selected impact resilience as the benchmark for determining mechanical efficacy. The overarching motivation behind amalgamating a relatively malleable material with a sturdier, yet more brittle compound is to augment the energy dissipation potential of these combined structures. This is achieved via deformation and layer separation processes in the more ductile material. We employed quasi-static indentation to evaluate the resilience of these composites under continuous stress. Additionally, drop-weight impact assessments were undertaken to discern the performance variances at different strain rates.

We delved into the impact attributes of two distinct material pairings. The initial combination comprises an epoxy/CF composite meshed with a PA6/recycled CF mat. Our prior discourse revealed that the PA6/epoxy pairing possesses the capability to generate adhesive EP-PA linkages that even surpass the inherent cohesion of EP-EP bonds. This ability is heavily reliant on processing nuances. In this matrix, the inherently malleable

PA undergoes both elastic and plastic transformations to dissipate energy, thereby safeguarding the more fragile epoxy from fracturing. Concurrently, the carbon fiber fortification in the PA imparts robustness, ensuring that the overall rigidity and resilience of the structure are not compromised in pursuit of enhanced impact resistance.

Another explored pairing encompasses aluminum integrated with PA6/recycled CF. Aluminum's appeal stems from its lightweight nature, malleability, and energy absorption attributes. Yet, its pronounced ductility renders it prone to superficial deformities from trivial collisions, making it less ideal for certain applications like automotive body panels where even minor disruptions can blemish its aesthetics. In stark contrast, composite layers exhibit a heightened resistance to such superficial impairments. This raises the potential of employing a slender composite layer, such as PA/CF, to preserve a sleek surface even upon minor impacts. As touched upon in our earlier discussion, PA has the intrinsic potential to bond with the alumina film present on the aluminum surface, eliminating the need for additional surface treatments to strengthen this bond.

It's worth noting that all PA/CF specimens examined herein were nonwoven matrices, composed of intertwined PA and reused carbon fibers. The random orientation and adequate length of these fibers ensure that these laminates emulate the behavior typical of quasi-isotropic continuous fiber reinforcements.

2. Crash Behavior in Heterogeneous Composites: The Interplay between Epoxy and Polyamide

Epoxy-based composites are progressively marking their footprint in high-end applications due to their impressive strength-to-weight ratio compared to conventional materials like steel. Nevertheless, the innate brittleness of epoxy poses challenges in contexts involving high impacts. A prevalent strategy to mitigate this shortcoming is the integration of a thermoplastic element within the composite.

Polyamide (PA) stands out in this category, largely owing to its chemical affinity with epoxide groups, offering an unparalleled compatibility amid thermoplastics [1][2]. This inherent cohesion paves the way for its deployment in an array of configurations, such as its dispersion in epoxy resins[3][4], intertwined fibers[5][6], or discrete particle[7]-[9] and veil[10]-[12] layers within composite architectures. Irrespective of its arrangement, the underlying mechanisms through which PA amplifies the composite's resilience are twofold: the debonding process at the interface and the PA phase deformation. The synergy between these two mechanisms underscores the vitality of the bond strength between PA and epoxy for efficient energy dissipation.

The balance between strength and flexibility is delicate: a subpar bond may curtail energy absorption by early debonding and hinder load transfer to the PA phase, suppressing its energy-dissipating deformations. On the other hand, an overly robust bond might lead to a premature failure of the composite, rendering it vulnerable[3]. Additionally, in certain use-cases, an exceedingly sturdy bond could potentially confine PA's energy-dissipating capabilities[4][5].

While thermoplastics enhance toughness, some studies indicate a potential compromise in the holistic performance of the composite. This stems predominantly from the reduction in fiber content, since the introduction of thermoplastics increases the composite's volume without proportionately amplifying its strength[6]. Occasionally, this can even supplant the reinforcing fibers[5]. Yet, designers often reconcile with this trade-off, integrating it into their design calculus. In an attempt to rectify these challenges, our research employs carbon fiber-reinforced PA, ensuring that composite robustness remains intact.

Literature suggests that augmenting composite laminates with tougher materials on their exposed surface can elevate their resistance to impacts[13]-[16]. This outer layer, being more ductile, efficiently disperses the stresses resulting from the impact. Moreover, a sturdy bottom layer is poised to counteract the tensile forces ushered in by impact-driven flexion. Our study meticulously assesses laminates with varied orientations to discern the veracity of these findings within our chosen material configurations.

2.1 Experimental Framework

Materials - The epoxy/carbon fiber (CF) composite deployed in our investigation was sourced as Cytec 977-2/IM7, an epoxy (EP) prepreg featuring unidirectional carbon fiber integration. Concurrently, the PA/CF material was procured as a nonwoven blend of PA6 and salvaged carbon fibers from ELG composites. Prior to utilization, the PA/CF was subjected to a consolidation process under a force of 10 tons at 270°C for a duration of 10 minutes. This was imperative, considering the disparity in processing temperatures between the epoxy and the PA6.

Sample Synthesis - Our samples comprised 8 layers of pre-processed PA/CF composite superimposed on 17 layers of unprocessed epoxy/CF, orchestrated in a cross-ply configuration, as depicted in Figure 1. These assemblies were molded using a heated press, facilitating the simultaneous curing of epoxy with the pre-processed PA/CF laminate. All specimens were subjected to a compression of 690kPa.

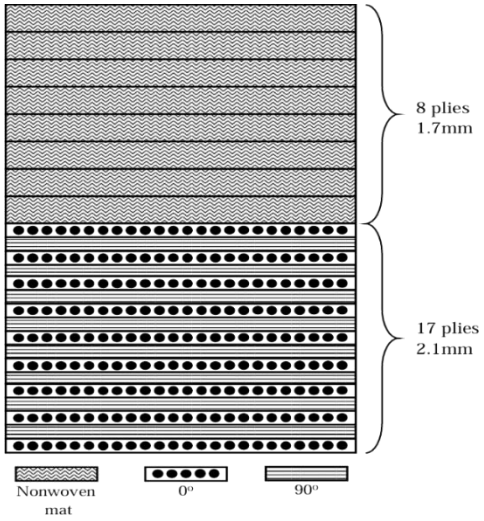

Figure 1. Illustration of the laminate stacking sequence. PA/CF layers are symbolized by undulating lines, while the orthogonal lines and circles denote the 0° and 90° epoxy/CF layers, respectively.

For our study, two distinct processing temperature and time pairs were selected – the factory-recommended 177°C for 3 hours and an elevated 197°C for 45 minutes. Past explorations using these parameters [17] highlighted an increase in fracture resilience at the epoxy/PA juncture by as much as 215% upon elevating the processing temperature from 177°C to 197°C. The nomenclature adopted for our samples is summarized in Table 1.

Table 1. Overview of sample orientation, processing parameters, and associated nomenclature.

Top Material	Bottom Material	Tproc (°C)	Sample Label
EP/CF	PA6/CF	177	EP/PA177, EP top
EP/CF	PA6/CF	197	EP/PA197, EP top
PA6/CF	EP/CF	177	EP/PA177, PA top
PA6/CF	EP/CF	197	EP/PA197, PA top

2.1.1. Mechanical Evaluation: Quasi-Static Indentation (QSI)

The QSI tests were conducted in line with the standards delineated by ASTM D6264[18]. Square samples measuring 63.5x63.5mm were securely positioned between steel blocks that had square openings of 50.8x50.8mm, as depicted in Figure 2.

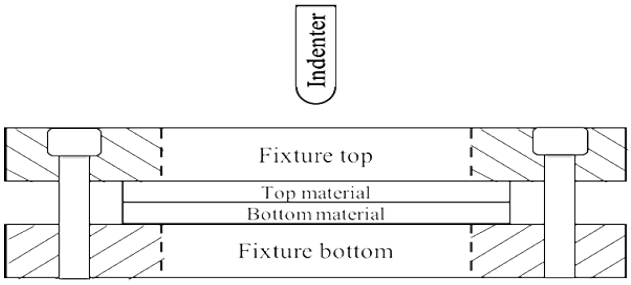

Figure 2. Apparatus for QSI and Drop-Weight Impact Analysis.

A steel rod, endowed with a hemispherical tip of 6.35mm diameter, was affixed to the top crosshead of a hydraulic testing apparatus. Each sample was subjected to a compression load, administered at a consistent displacement pace of 1mm/min, until the impactor completely permeated the sample. Throughout this process, both the exerted force and the displacement of the crosshead were meticulously recorded.

The energy dissipated during the loading phase was determined using the following equation[18]:

\[E_{abs} = \int_{\delta_0}^{\delta_f} F(\delta) \, d\delta \]

\[Equation \: [4.1] \]

2.1.2. Mechanical Evaluation: Drop-Weight Impact Assessment

For drop-weight impact analysis, procedures outlined by ASTM D7136[19] were followed. A 2.5kg steel rod, equipped with a hemispherical tip measuring 6.35mm in diameter, was allowed to fall freely within a confined column from varying elevations, generating impact energies spanning from 10-22J. These falls corresponded to impact speeds ranging between 7-10.5m/s. The imparted energy was adjusted in accordance with the sample thickness using the formula:

\[E = CE \times h \]

\[Equation \: [4.2] \]

Here, \(h \) symbolizes the sample's thickness in millimeters and \(CE \) denotes a pre-decided ratio of the impact energy to the sample's thickness (expressed in J/mm).

Selected \(CE \) values ensured sub-critical energy impacts, meaning the impacts didn't penetrate the samples. These ranged from 2.7-5.7J/mm, corresponding to energies between 10-22J and velocities of 7-10.5m/s.

Sample placements were consistent with Figure 2's schematic. Rebound heights, post-impact, were captured with a strategically placed camera, and the resulting dent's depth on the sample was gauged immediately.

The energy absorbed by the sample was deduced using the equation:

\[E_{abs} = m \times g \times (h_0 - h_f) \]

\[Equation \: [4.3] \]

Where:

- \(m \) = mass of the impactor

- \(g \) = gravitational acceleration

- \(h_0 \) = initial height of the impactor

- \(h_f \) = final rebound height of the impactor

This assessment presumes that all imparted energy was either stored by the sample or transmuted into rebound energy, intentionally sidelining losses due to variables such as internal drop tower friction or atmospheric resistance. However, this approximation was deemed acceptably accurate for the scope of this work.

Lastly, to enable more equitable comparisons across diverse impact energies, the percentage of energy absorption was ascertained. This was merely the fraction of the initial energy that was absorbed by the sample during the impact.

2.1.3. Mechanical Evaluation: Non-Destructive Imaging via 3D X-ray Microscopy

To scrutinize the intrinsic damage resulting from impact events, we employed a Zeiss Xradia 510 Versa 3D X-ray microscope. Images were obtained using an 80V power source, with a brief exposure duration of 0.5 seconds. Each individual scan yielded a series of 1012 images, each possessing a pixel granularity of 55.59µm. Following acquisition, VGSTUDIO MAX was used for the reconstruction and in-depth damage analysis.

Delamination extents were initially gauged using VGSTUDIO MAX's crack segmentation tool, which capitalized on grayscale variances to demarcate probable damage zones. This is depicted in Figure 3, where the blue contour demarcates the region of interest (ROI). This delineated area was extracted as a mask for defect identification, subsequently utilized

for a porosity analysis, facilitating the recognition of delamination volumes. The damage volume's projected area, orthogonal to the impact plane, was employed to determine each sample's delamination area.

Yet, for samples exhibiting minor damage, the crack segmentation approach proved insufficient. For such instances, crack segmentation was supplanted with grayscale thresholding, supplemented by manual removal of intrinsic material porosity. The ROI results were visually analogous to those displayed in Figure 3, though this alternate method ameliorated sensitivity to innate material density deviations that weren't indicative of damage.

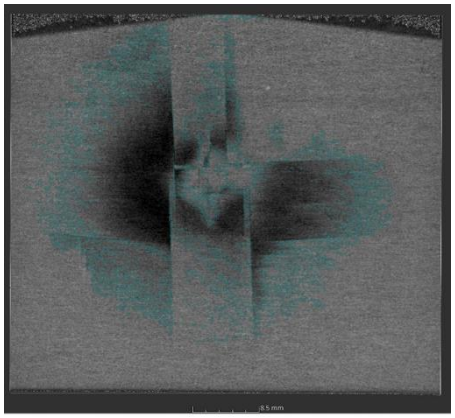

Figure 3. Depiction of the identified defect ROI via the crack segmentation tool, suggesting regions with heightened damage probabilities.

2.2 Results and Analysis

2.2.1. Quasi-Static Indentation (QSI)

Characteristic force-displacement profiles are showcased in Figure 4 for each sample group.

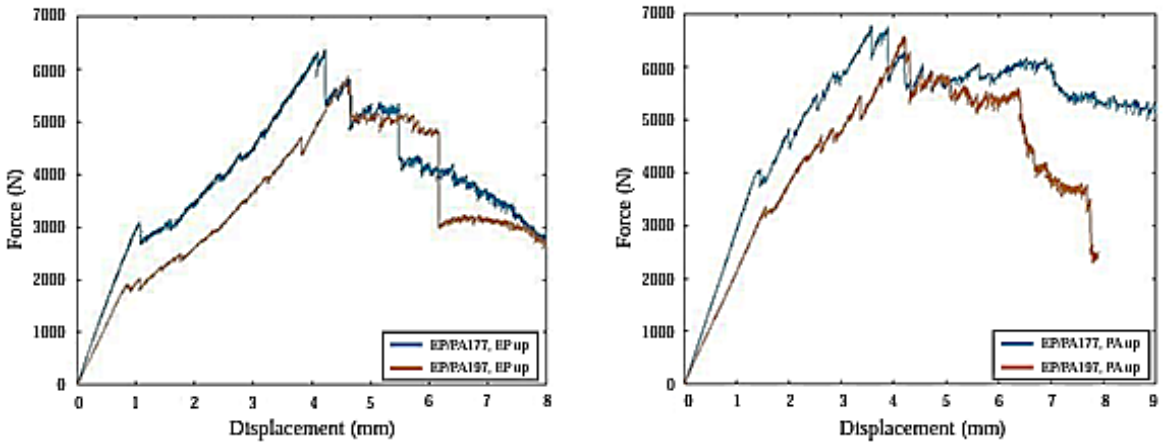

Figure 4. Distinctive force-displacement trajectories for EP-up (left) and PA-up (right) samples.

Initial failure points, denoted by the digression from the load curve's linearity, seemed indifferent to processing temperatures. Interestingly, the PA-up samples sustained heftier loads prior to witnessing their first failure, implying an advantage in PA-up configurations when early failure serves as a critical design determinant. This was likely attributed to the PA/CF's enhanced malleability, offering effective dispersion of low-energy contact stresses.

However, the most critical criterion in gauging crash performance is the sample's sustained load-bearing capacity post the primary failure. Amongst the cohorts, EP/PA197 samples with the PA orientation up emerged superior. A myriad of factors converged here, from the ductile upper layer dissipating stresses to the sturdier lower layer countering tensile stresses elicited due to out-of-plane flexure during evaluation. The robust EP-PA boundary further fortified this, ensuring that, despite high out-of-plane displacements, load transfer persevered.

Figure 5 offers a visual of the apex loads each sample variety experienced, averaged across all evaluated specimens.

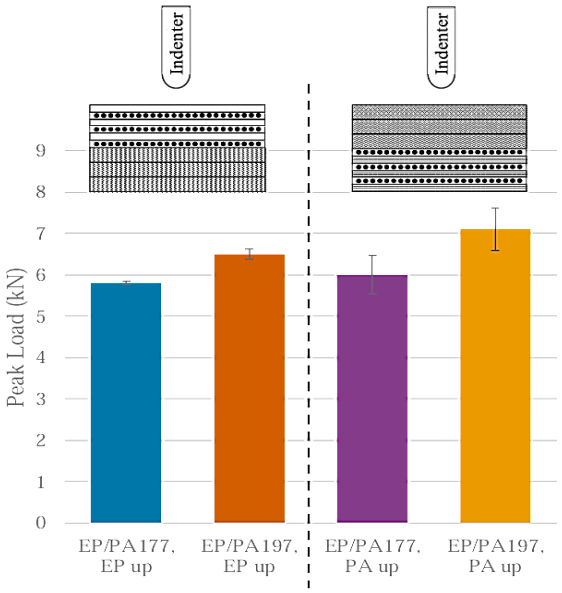

Figure 5. Peak loads registered during the QSI evaluations.

Figure 6 visualizes the energy absorbed during tests, averaged per sample category.

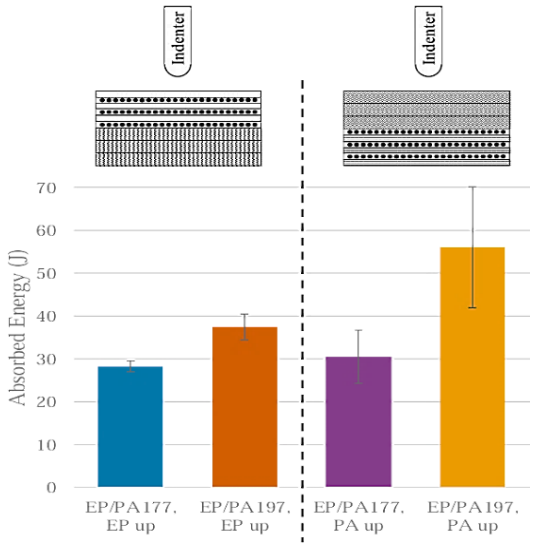

Figure 6. Energy absorbed by the samples through QSI evaluations.

Observations indicated a prominent variability amongst PA-up samples compared to their EP-up counterparts, possibly arising from the juxtaposition of a compact plate size against the considerable anisotropy native to the PA6/CF nonwoven mat. Despite these discrepancies, EP/PA197 samples with PA facing upwards unequivocally outperformed their counterparts in QSI assessments, attributable to a trio of synergistic factors: effective stress dispersion by the ductile PA/CF layer, heightened resistance to impact-induced bending from the stronger EP/CF, and sustained load transfer despite damage progression due to the robust EP-PA interface. This confluence of advantages translated into a whopping 98% surge in absorbed energy, merely by modifying processing temperature and inverting part orientation.

2.2.2. Drop-Weight Impact Assessment

The resultant depth of dents post-impact, as illustrated in Figure 7, adheres to the guidelines specified by ASTM D7136. Remarkably, irrespective of variations in processing temperature or component orientation, the dent depths were consistently minor, hovering around or even below the sensitivity benchmark of 0.25mm. This implies that discernible surface deformations, in scenarios involving low-intensity impacts, aren't a pressing concern for components synthesized from this material combination, irrespective of their orientation with respect to the impacting object.

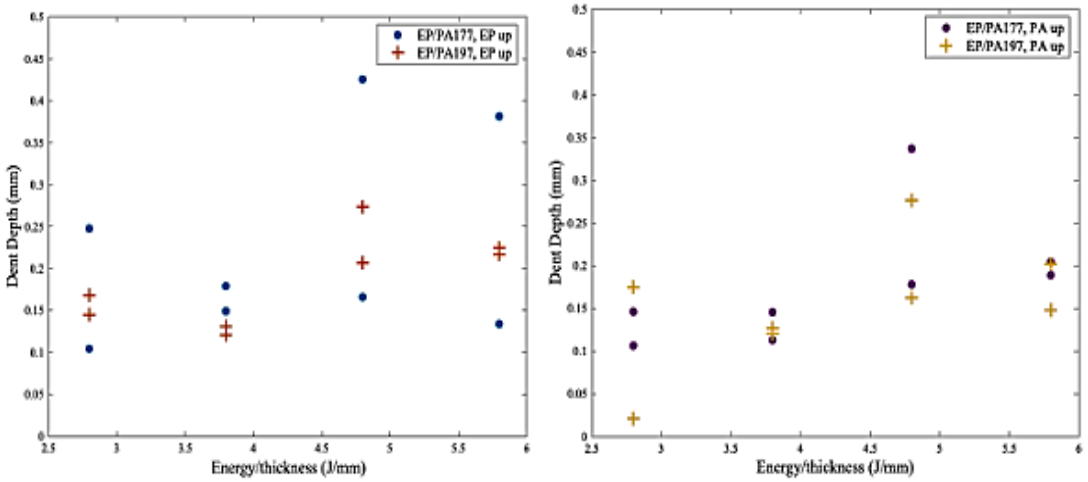

Figure 7. A comparative assessment of the dent depths immediately post-impact: left showcases the aftermath of impacting the epoxy surface, whereas the right focuses on the polyamide surface.

Figure 8 provides a visual representation of the proportion of imparted impact energy that was absorbed by the specimens. In scenarios where the epoxy surface faced the brunt of the impact, the energy absorption rate for EP/PA197 samples showcased a level of consistency, regardless of the escalation in impact energy. In stark contrast, the EP/PA177 samples exhibited a pronounced spike in absorbed energy percentages between the E/h values of 3.8 and 4.8. This dramatic ascent could potentially be indicative of a delamination threshold being met within this energy interval, a hypothesis resonating with the findings of Nixon et al. [20].

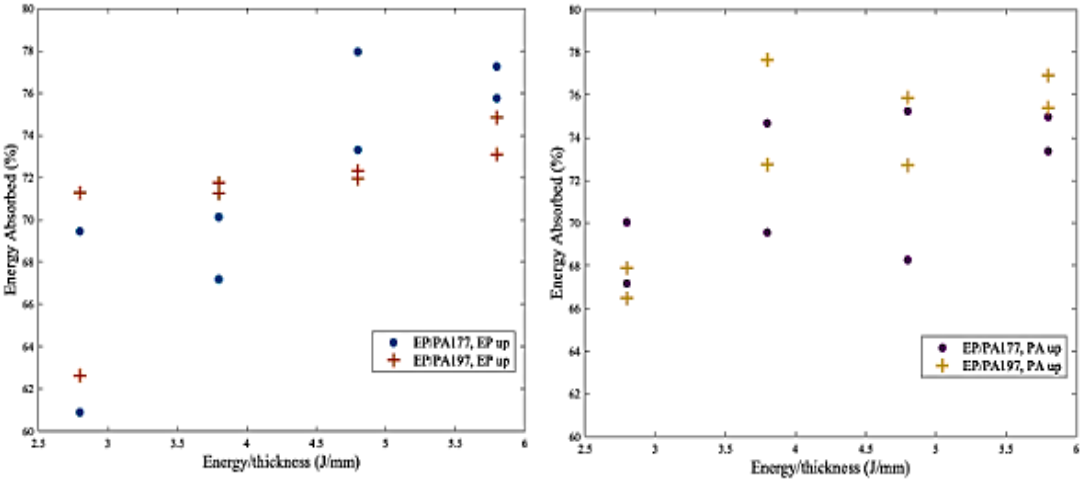

Figure 8. Graphical depiction of the percentage of energy absorbed during drop-weight impact testing: left pertains to instances where the epoxy surface absorbed the impact, while the right depicts the results from the polyamide surface.

The behavior exhibited by the PA-up samples appeared more erratic. The two distinct processing temperatures, surprisingly, didn't offer statistically significant differentiation in outcomes. One could conjecture that this could be a consequence of the sporadic arrangement of carbon fibers on the impacted surface coupled with the compactness of the plate dimensions. Such a combination could render the plates more susceptible to inherent, local material inconsistencies.

2.2.3. Further Analysis on Drop-Weight Impact Assessment

a. Internal Damage Assessment

To provide a more in-depth understanding of the impact effects, the internal damage mechanisms were also considered. While the surface dents were minimal, internal delaminations or fiber breakages could compromise the structural integrity of the component in the long run.

Using non-destructive imaging techniques, such as ultrasonic C-scanning or CT scanning, would offer insight into the extent and nature of internal damages. This would also provide a clearer picture of the actual resistance of these materials against impact loads.

b. Variability in the PA-up Samples

The inconsistency observed in the PA-up samples could be further explored. The random orientation of the carbon fibers on the impacted surface suggests a more complex stress distribution during the impact. This randomness, while offering isotropic properties in the material, may also lead to unpredictable energy absorption patterns during an impact. The fiber-matrix interface, fiber orientation, and inherent defects in the PA layer could play significant roles in determining the energy absorption capabilities.

It might be beneficial to study larger sample sizes to minimize the influence of local material inconsistencies. Furthermore, a detailed microstructural analysis, focusing on the fiber-matrix bond quality, could shed light on potential weak points that contribute to the observed variability in the PA-up samples.

c. Comparison with Other Hybrid Systems

While the current study focuses on the epoxy and polyamide system, it would be worth comparing these results with other hybrid systems, especially those used in similar applications. Such comparisons would help in determining the relative advantages and limitations of the epoxy-polyamide system over its counterparts.

d. Practical Implications

In real-world scenarios, components might not be subjected to perfectly perpendicular impacts. Therefore, assessing the impact resistance under different angles of impact would be valuable. This would simulate more realistic conditions, such as oblique impacts, which often occur in automotive or aerospace accidents.

2.2.4 Overview of CT Analysis

Leveraging the capability of Computed Tomography, we delved into the internal structure of impacted samples. The results, displayed in Table 2 and encapsulated visually in Figure 9, revealed the delamination area, particularly occurring between the EP layers and at the EP-PA junction. Given the amalgamation nature of the PA/CF nonwoven mats during compression molding, distinct laminae were not discernible. This probably stems from the interplay of nonwoven carbon fibers across ply interfaces, confining the delamination primarily to the EP/CF material.

The progression of delamination typically followed the carbon fiber orientations, manifesting largely in diamond-shaped regions due to its spread along the 0° and 90° directions. In instances where delamination reached the sample boundaries, the resulting damage regions bore a more irregular shape.

The PA/CF structural impairments were predominantly elusive at the scanning resolutions deployed. However, any discernible damages appeared as linear matrix fissures extending along the 0° and 90° orientations.

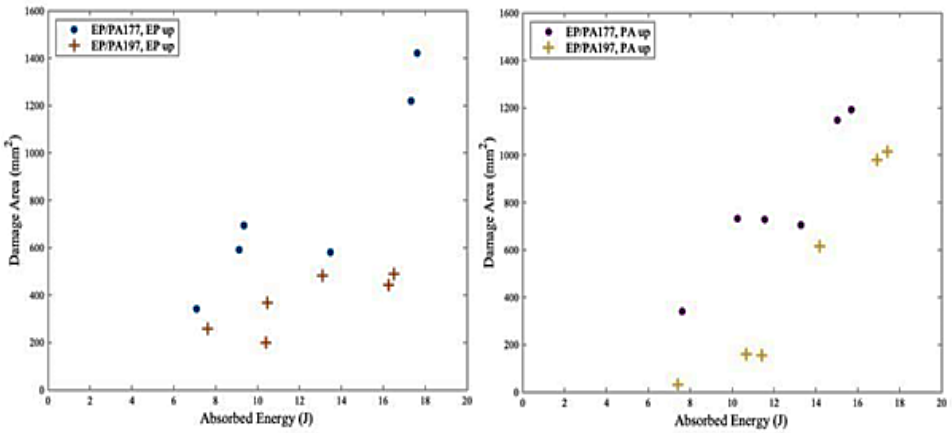

Figure 9. Projected damage swathes in drop-weight impacted samples. The left spectrum represents EP-up samples, whereas the right portrays PA-up samples. Here, damage areas are juxtaposed with impact-induced energy absorption.

Table 2. Illustrative damage areas derived from CT scans post-impact.

	Impact Energy (J/mm)				
	2.8	3.8	4.8	5.8	Projected x-y damage area (mm2)
EP/PA 177, EP up	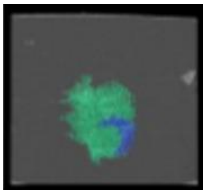	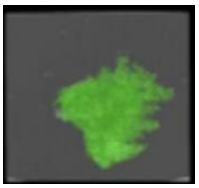	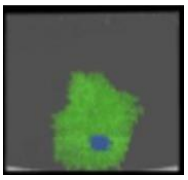	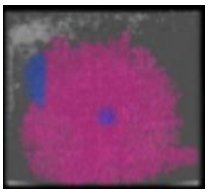	
EP/PA 177, PA up	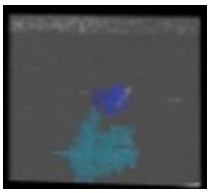	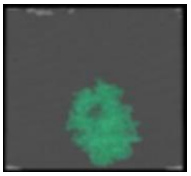	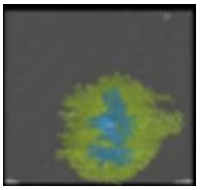	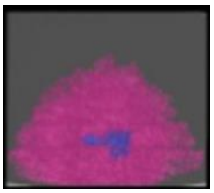	
EP/PA 197, EP up	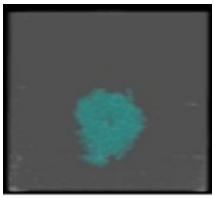	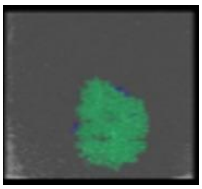	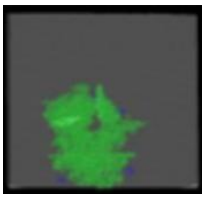	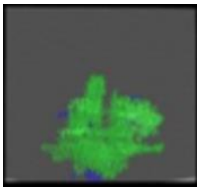	
EP/PA 197, PA up	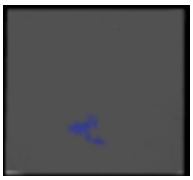	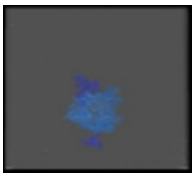	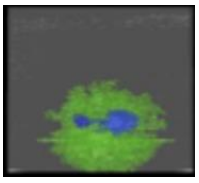	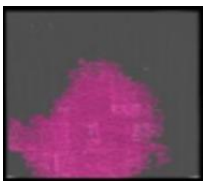	

2.3 Insights from Damage Patterns

For all specimen orientations, it was evident that samples with frailer EP-PA boundaries had more extensive damage realms. A substantial increment in damage zones was noted when the imparted impact energy transcended a particular threshold, linking with the escalation in E/h from 4.8 to 5.8 J/mm. This suggests the surpassing of damage initiation or propagation limits at this energy juncture. Remarkably, the EP/PA197, PA up samples depicted steady damage areas even upon this energy enhancement, implying heightened delamination resistance within the tested energy spectrum.

2.3.1 Concluding Remarks

The amalgamation of epoxy and polyamide matrix composites into hybrid composites via spontaneous adhesion during compression molding has borne significant findings:

1. The EP-PA bond strength, modulated through processing temperature nuances, exerted pronounced influence over the hybrid's resilience against impacts.

2. In the presence of weaker EP-PA bonds, part orientation scarcely affected impact resistance, whether gauged through drop-weight or QSI methodologies.

3. Delamination thresholds were discernible, beyond which extensive structural impairment ensued. Enhancing bond robustness could potentially elevate this threshold.

4. The application intent for EP-PA hybrid components will invariably influence the optimal orientation. For instance, while the PA-up orientation showcased superior crash endurance, the EP-up demonstrated improved resistance against delamination in specific energy ranges.

5. Subsequent research might explore the ramifications of broader sample dimensions, alleviating fixture-induced constraints, and a more diverse spectrum of impact energies to ascertain the penetration resilience of EP-PA hybrids.

3. Performance Analysis of Hybrid Materials: Aluminum and Recycled Thermoplastic Composite

Aluminum is frequently favored in applications demanding lightweight characteristics, even at the cost of comparatively lesser strength. Its weldability ensures seamless integration into prevailing manufacturing processes, facilitating high-speed production. Such attributes render aluminum an optimal material for automobile components. Nonetheless, aluminum's pronounced ductility renders it vulnerable to superficial dents—common challenges faced during a vehicle’s operational lifecycle, including damages from hailstones and road debris.

Contrastingly, composite materials are renowned for their resilience against superficial damages. When the composite's primary role is to resist minor surface abrasions without the necessity to endure intense impacts, concerns over latent internal damages become secondary. Additionally, composites employing thermoplastic matrices, particularly polyamide (PA), are equipped to better dissipate impact energies. This advantage stems from thermoplastics' intrinsic capacity to undergo elastic deformations when subjected to external forces.

The crux of this research pivots on assessing the impact resistance of hybrid constructs, conceived by amalgamating aluminum with a PA-based composite reinforced with recycled carbon fibers. Benchmarks are set through comparisons with their homogeneous aluminum and composite counterparts to elucidate the implications of this hybridization. The rationale behind combining rather than substituting aluminum with composite material lies in the facilitation of integration into conventional methods. For instance, the exposed edges of aluminum could seamlessly be welded. Moreover, introducing a composite constituted from recycled carbon fibers serves to validate the potential of repurposed fibers in contexts demanding impact resistance. The resultant hybrid construction postulates an eco-friendly profile, asserting a reduced carbon footprint.

Crucially, the methodology employed champions the spontaneous adhesion between polyamide and aluminum. While literature abounds with strategies to enhance this adhesion, most either necessitate exorbitant apparatus [23]–[27], resort to deleterious chemicals [28]–[31], or impose additional processing overheads. Such complexities compromise their applicability in high-frequency production scenarios. Nevertheless, it merits acknowledgment that a fortified interfacial bond might further augment the impact resistance of hybrid constructs by facilitating superior load distribution and amplifying the energy needed for debonding. While this concern remains secondary when employing composites to fortify aluminum surfaces against low-intensity impacts, it escalates in significance when the goal is to leverage aluminum-composite hybrids for elevated crash resilience. In such contexts, strategies geared towards reinforcing adhesion show promise.

3.1 Experimental Approach: Aluminum and Recycled Thermoplastic Composite Integration

3.1.1 Materials and Design

The subject under scrutiny comprised sample plates that manifested either as standalone aluminum plates, solitary composite laminates, or an amalgamation of the two, elucidated in Figure 10. Two distinct thicknesses of Aluminum 3003, specifically 0.4mm and 2mm, were employed in the fabrication of the aluminum plates.

Figure 10 showcases the different material configurations for this investigation. The designs varied from pure aluminum plates to composite laminates, and intriguing combinations thereof.

The composite material chosen was an intertwined PA6/CF nonwoven mat that had commingled PA6 fibers amalgamated with recycled carbon fibers. A uniform thickness, close to 2mm, was pursued to enable a facile comparison between the composite and aluminum. To ensure optimal consolidation, the nonwoven mat layers were desiccated at 80°C for a span of 4 hours. This was immediately followed by compression molding them under 690kPa at a temperature of 270°C for 10 minutes.

3.1.2 Sample Synthesis

To initiate, every aluminum plate had one of its surfaces abraded, purified, and subsequently coated with a gentle etchant to act as a cleaning medium. This measure was to prohibit any alien substances from compromising the bond's integrity.

Subsequently, the aluminum was methodically positioned in a 254mmx254mm mold, ensuring the purified surface was oriented upwards. A pre-settled PA6/CF laminate was layered onto the aluminum. Under the specified pressure and temperature conditions, the assembly underwent compression and was then allowed ambient cooling. A comprehensive overview of the prepared samples can be perceived in **Table 3**. The tabulation aims to group the samples to pave the way for intuitive comparisons.

Table 3. encapsulates a snapshot of the combinations of aluminum and PA6/CF hybrids that were chosen for the quasi-static indentation and the drop-weight impact evaluations.

Impacted Material	Bottom Material	Label	Sample Group
PA6/CF mat, 8 plies	N/A	PA	
0.4mm-thick aluminum	N/A	0.4mm Al	Thin Aluminum
0.4mm-thick aluminum	PA6/CF mat, 8 plies	Thin hybrid, Al up	Thin Aluminum
PA6/CF mat, 8 plies	0.4mm-thick aluminum	Thin hybrid, PA up	Thin Aluminum
2mm-thick aluminum	N/A	2mm Al	Thick Aluminum
2mm-thick aluminum	PA6/CF mat, 8 plies	Thick hybrid, Al up	Thick Aluminum
PA6/CF mat, 8 plies	2mm-thick aluminum	Thick hybrid, PA up	Thick Aluminum

For the experimental phase, each comprehensive plate was meticulously subdivided into sixteen squares, each measuring 63.5mm x 63.5mm, via waterjet cutting to negate the potential for localized melting or inadvertent edge damages.

3.1.3 Mechanical Analysis: Drop-Weight Impact Assessment

To discern the susceptibility of the samples to low-velocity impacts, drop-weight impact testing was orchestrated, adhering to ASTM D7136 guidelines. An impactor, fabricated from steel and weighing 0.55kg, possessing a 6.35mm diameter hemispherical tip, was released from calculated altitudes to manifest diverse impact energies. The stark disparity in sample thicknesses, oscillating between 0.4mm to 4mm, necessitated a pre-defined ratio of impact energy concerning sample thickness, spanning from 0.8 to 4.8 J/mm. Post-impact, the depth of the dents was ascertained on the top surfaces.

3.1.4 Mechanical Analysis: Quasi-Static Indentation Testing (QSI)

In this approach, a hemispherical-tipped steel impactor, 6.35mm in diameter, was methodically pushed into the hybrid plate's expanse at a steady pace of 1mm/min. The consequent force and the crosshead displacement data were registered, facilitating the derivation of energy absorption during the QSI test phase. The detailed setup is pictorially presented in Figure 11.

3.2 Results

3.2.1 Drop-Weight Impact Testing

The rigorous testing for the PA and the PA-up hybrid samples unveiled a marked vulnerability to penetration at impact energies surpassing 1.8 J/mm. Consequently, subsequent to this threshold, dent depth data becomes unavailable. Through a meticulous dissection of the thin Aluminum sample group's impact performance, evident from Figure 10, certain critical insights emerge:

1. The dent depth in the PA-up hybrid samples consistently surpassed that in the PA samples. This phenomenon is attributed to the proclivity of the 0.4mm-thick aluminum, situated at the PA-up hybrid samples' base, to sustain enduring deformation post-impact. The bond strength between the aluminum and the PA6 showcased commendable resilience, leading to the PA6/CF at the hybrid samples' summit adopting the permanent deformation contours of the aluminum.

2. Relying solely on dent depth to anticipate material failure may be misleading, especially in the realm of composite materials. A stark manifestation of this can be seen where, despite the PA and PA-up hybrid samples registering lesser dent depths compared to the 0.4mm Al and Al-up hybrid samples, both the PA and the PA-up hybrid samples underwent penetration at a substantially lower energy to thickness ratios.

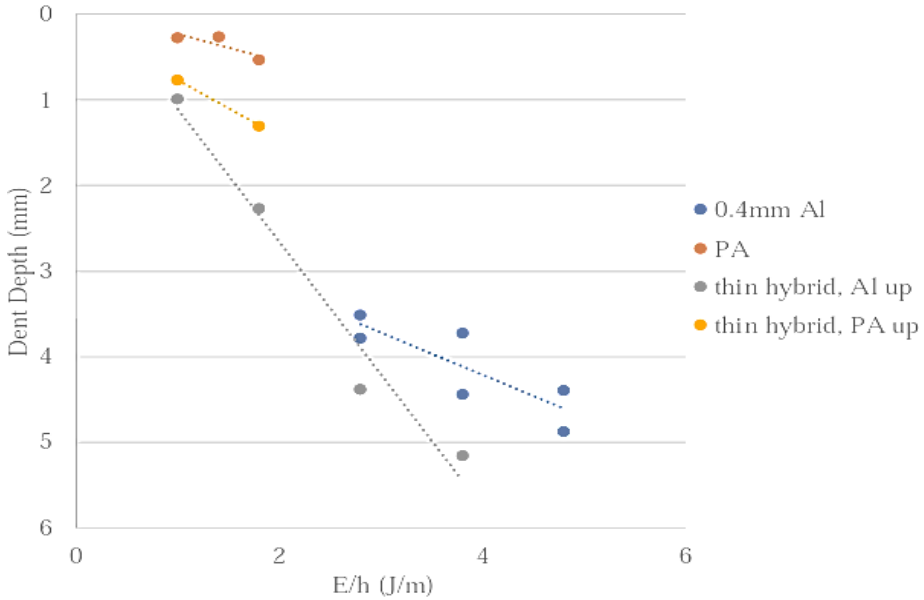

Figure 10. offers a visual representation of dent depths observed upon subjecting thin Al/composite hybrid samples to low-velocity impacts.

Expanding our analytical horizon to the Thick Aluminum sample group (in alignment with the delineations in **Table 3**), we unearth a new set of observational data, graphically showcased in Figure 11. The discerning insights encapsulated from this subset include:

1. At the foundational impact energy levels, the PA and PA-up hybrid samples exhibited a remarkable semblance, marked by an inconsequential variation in dent depth.

2. An intriguing observation surfaces wherein the PA samples suffered full penetration post hitting an energy to thickness ratio of 1.8 J/mm. In stark contrast, the PA-up hybrid samples exhibited a stalwart resistance, withstanding an augmented relative load by nearly 50%, post the aforementioned threshold. This revelation underscores the symbiotic impact of aluminum on these hybrid plates.

3. Diving deeper, it's evident that the extensive deformation of the bottom aluminum surfaces of these thick PA-up hybrid samples, in contrast to their top PA counterparts, hints at potential localized debonding at the epicenter of these samples between the aluminum and PA6/CF under the indenter's influence. Yet, this debonding phenomenon remains confined to the sample's core.

4. A pronounced surge in dent depth in the Al-up hybrid samples, particularly evident between the 1.4 and 1.8 J/mm brackets, is indicative of an almost exhaustive delamination between the aluminum and the PA6/CF composite in the 1.8 J/mm sample. This culmination implies that the aluminum, now unshackled on the surface, is at liberty to deform, absorbing the residual impact energy, thereby leading to a substantial dent depth escalation.

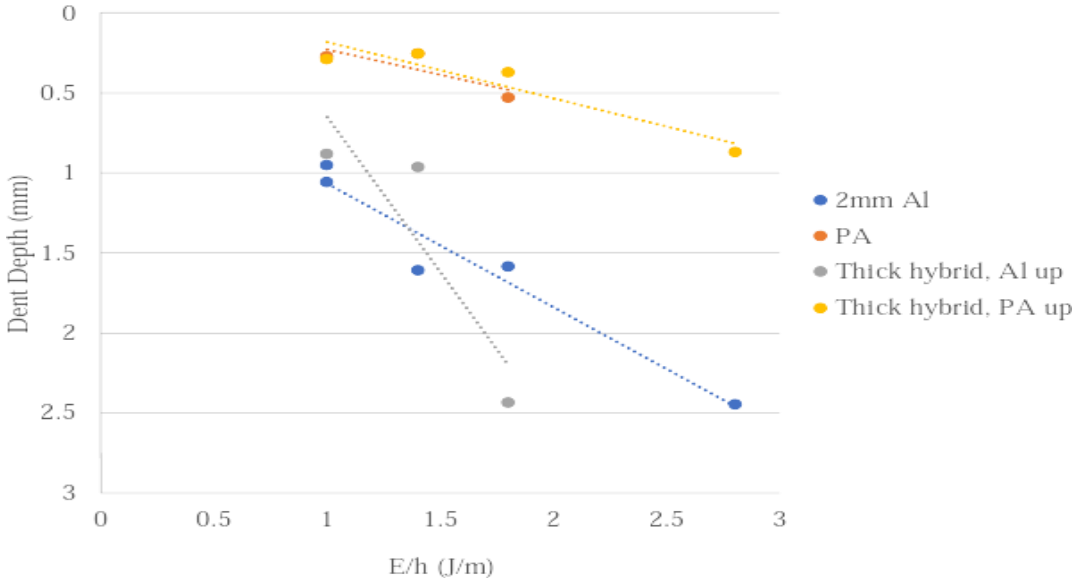

Figure 11. provides a pictorial narrative of dent depths recorded upon subjecting thick Al/composite hybrid samples to low-velocity impacts.

3.2.2 Quasi-Static Indentation (QSI) Results

a. Thin Aluminum Sample Group

Upon observing the force-displacement curves from QSI tests for the thin aluminum group of samples, shown in Figure 12, the following key insights emerge:

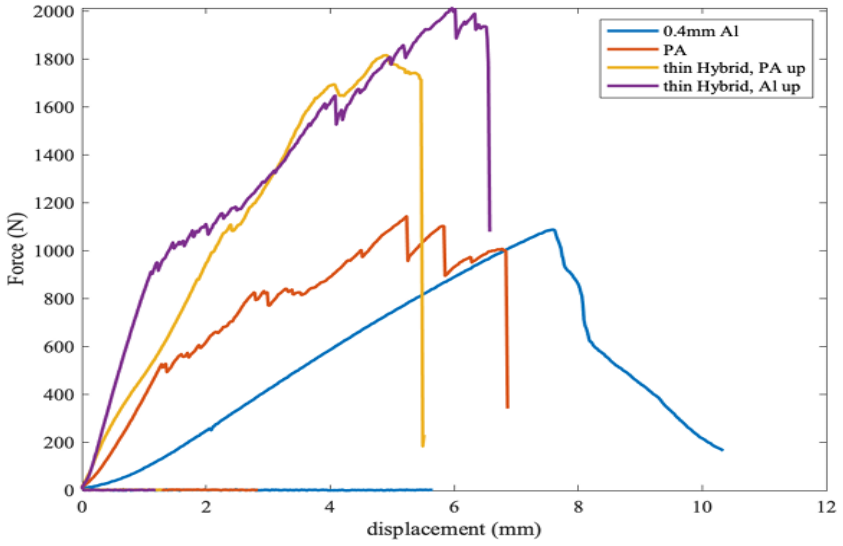

Figure 12. force-displacement curves from QSI tests for the thin aluminum group of samples

1. The PA6/CF composite without the aluminum component displays a brief initial linear phase. The first departure from linearity pinpoints the initial matrix fracture within the composite. Following this, the subsequent declines in the force-displacement curve signify progressive failures within the composite. These failures can manifest as matrix fractures, deformations between the matrix and fiber, or direct fiber fractures.

2. Hybrid samples of aluminum and composite indicate a pronounced reliance on which side the indenter impacts. Specifically:

When the aluminum side bore the brunt of the impact, the initial load curve steepened, signaling a stiffer load response compared to impacts on the PA6/CF side.

With the aluminum as the impact recipient, the load peak was notably heightened, and the indenter's maximum displacement prior to penetration was more pronounced.

In contrast, the initial fracture in samples with the PA6/CF side up occurs at almost double the initial displacement seen in the Al-up samples.

Table 4. catalogs the peak load and the energy absorbed during the QSI testing cycle for the thin aluminum sample group.

	PA/CF	0.4mm Al	Thin PA-up hybrid	Thin Al-up hybrid
Peak Load (kN)	1.14	1.09	1.82	2.01
Absorbed Energy (kJ)	4.89	4.54	5.98	8.50

b. Thick Aluminum Sample Group

Moving on to the thicker aluminum sample group, shown in Figure 13, we can distill the following interpretations:

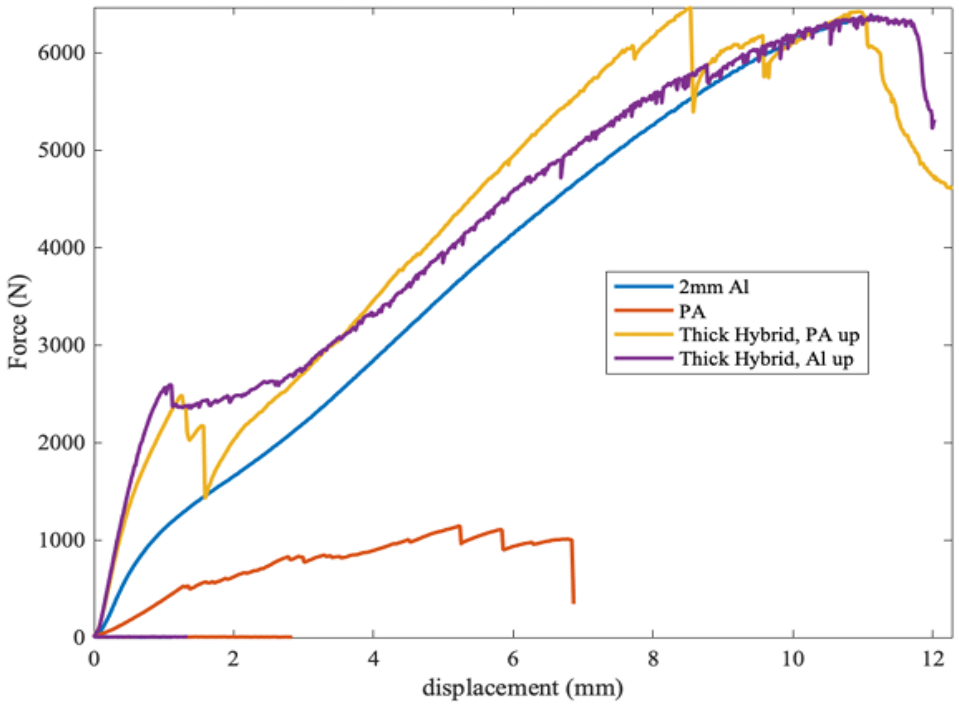

Figure 13. force-displacement curves from QSI tests for the thick aluminum group of samples

1. The pure aluminum samples reveal a deviation from linearity fairly early, marking the commencement of plastic deformation. This suggests that in these samples, most of the applied load is accommodated through plastic deformation.

2. The behavior of the hybrid samples was fairly consistent irrespective of the impacted face—whether aluminum or PA6/CF. However, some nuances were observed:

In Al-up samples, the load curve typically remained smooth with only minor depressions throughout the load cycle.

Conversely, the PA-up samples showcased significant load reductions along the curve, indicative of large-scale composite failures.

3.3 Discussion on Crash Performance of Aluminum/Recycled Thermoplastic Composites

The combination of aluminum and PA6/CF composites offers some unique mechanical behaviors when subjected to impact and quasi-static loads. The study underscores several critical findings:

1. Enhanced Impact Performance: The PA6/CF effectively minimizes visible surface damage during low-energy impacts. In combination with a thick aluminum base, this composite structure shows a pronounced resistance to penetration. This mutual enhancement highlights the synergy of combining these two materials.

2. Load Behavior of Hybrids: In quasi-static indentation tests, pure aluminum samples demonstrate smooth force vs. displacement curves, attributable to the homogeneity of the aluminum material. In stark contrast, the presence of PA6/CF in the samples introduced an initial linear region, succeeded by a jagged curve, post the initial internal failure within the composite.

3. Performance Improvements with Aluminum: The addition of even a thin layer of aluminum, either on the top or bottom of the PA6/CF composite, brought forth noticeable improvements in peak load-bearing and energy absorption. This surpasses the capabilities of both the standalone aluminum and the PA6/CF composite. The reason can be attributed to the significant energy absorption capacity of aluminum during its plastic deformation under these test conditions.

4. Complexities in Scaling Impact Results: The venture of scaling impact results of composites by thickness is intrinsically challenging due to the varying ply interfaces' behavior. The current study simplifies this by maintaining a constant number of composite interfaces, regardless of the sample's thickness, making the scaling by thickness approach valid for this discussion.

5. Superior Performance of Hybrid Samples: When scaled by thickness, the hybrid samples' results consistently eclipse the performance of pure PA6/CF samples. This emphasizes the potential advantages of integrating a thin layer of aluminum with the composite material.

6. Bonding Dynamics: The present bonding mechanism between aluminum and PA6/CF seems adept at managing both stress transfer and facilitating crack propagation. While there are multiple ways to enhance this bond, one must ponder if stronger bonding might inadvertently diminish the hybrid structure's energy absorption qualities. For instance, a very robust bond might restrain the aluminum's innate ability to undergo large-scale plastic deformation, a primary mechanism for energy dissipation.

To reach a more comprehensive understanding, future work could delve into the performance of hybrid composites with augmented interfacial bonds. Exploring the balance between bond strength, energy absorption, and material deformation could pave the way for optimized hybrid material designs for specific applications.

3.4 Recap of the Aluminum/PA-Based Composite Crash Performance

In this section, the beneficial synergies between aluminum and PA-based composites in the context of static and dynamic impacts were explored. Let's distill the key takeaways:

1. Improved Impact Behavior: Integrating an aluminum sheet with a PA-based composite markedly bolsters its performance during static and dynamic impacts. The aluminum's inherent properties, combined with the PA/CF composite's characteristics, create a material that excels in both static and dynamic loading conditions.

2. Complementary Performance: The presence of the PA/CF laminate does not diminish the aluminum's static performance. Conversely, the PA/CF composite benefits from the aluminum backing during impacts. When the composite side faces the impact, dents are noticeably reduced compared to when the aluminum side is exposed. Aluminum, being highly ductile, is more prone to denting, a problem alleviated by the protective PA/CF laminate.

3. Applications: The hybrid structure appears ideal for applications where aluminum is expected to bear significant impact loads. The added PA/CF laminate serves to shield the aluminum from minor impacts, thereby maintaining the part's visual appeal. For instance, in automotive applications, where aesthetics are paramount and minor impacts like stone chips or hail are commonplace, such hybrid materials can be invaluable.

4. Adhesion Dynamics: The present study underscores that the existing adhesion between the aluminum and PA-based composite is sufficiently robust to bear impact loads without causing extensive interface failures. However, there's a delicate balance to maintain. Increasing the bond's strength might inadvertently reduce the material's ability to absorb impact energy. The localized debonding at the impact site, as observed, acts as a vital energy-dissipating mechanism. Strengthening the bond could rob the hybrid of this mechanism, potentially leading to premature failures in the aluminum or the composite layer.

3.5 Summary

This chapter dives deep into the behavior of hybrid materials under different impact conditions, elucidating the importance of material combinations and the role of interfaces. Let's summarize the salient points:

1. Surface Protection: Composite laminates offer a potent shield against surface denting in low-energy impacts, unlike aluminum which is prone to such damage. Hence, composite materials are effective for protecting materials susceptible to superficial dents.

2. Optimal QSI Behavior: For the most effective energy absorption in quasi-static indentation, it's beneficial if the top material has higher ductility (to dissipate stresses) while the bottom layer exhibits superior yield strength (to resist impact-induced bending).

3. Mutual Benefits in Impact: The hybrid plates demonstrated a reciprocal advantage during drop-weight impact tests. Regardless of the material first exposed to the impact, these hybrid systems performed admirably.

4. Delamination Threshold: Delamination between the hybrid materials happens once a certain impact energy threshold is reached. However, enhancing the bond strength between the materials can raise this threshold, offering resilience to even higher impact energies.

5. Hybrid Design is Crucial: A good interface in hybrid materials is vital for optimum crash performance. Furthermore, designing the material system correctly can ensure maximum energy absorption during impacts.

The chapter establishes the significance of judiciously designing hybrid material systems for optimal crash performance. It emphasizes not just the choice of materials but also the design of their interface.

Acknowledgements

The support and contributions from ELG Composites, Dr. Joshua Dustin, Thomas Beimrohr, and Chven Mitchell were invaluable for this research. The advanced imaging provided by the Zeiss Xradia 510 Versa 3D X-ray Microscope, backed by Purdue University's EVPRP Major Multi-User Equipment Program 2017, enriched the study's findings.

References

[1] R. B. Prime and E. Sacher, “Kinetics of epoxy cure: 2. The system bisphenol-A diglycidyl ether/polyamide,” *Polymer*, vol. 13, no. 9, Sep. 1972, https://doi.org/10.1016/0032- 3861(72)90113-9

[2] Z. Zhong and Q. Guo, “Miscibility and cure kinetics of nylon/epoxy resin reactive blends,” *Polymer*, vol. 39, no. 15, Jul. 1998, https://doi.org/10.1016/S0032-3861(97)10237-3

[3] C. Girodet, E. Espuche, H. Sautereau, B. Chabert, R. Ganga, and E. Valot, “Influence of the addition of thermoplastic preformed particles on the properties of an epoxy/anhydride network,” *Journal of Materials Science*, vol. 31, no. 11, pp. 2997–3002, Jun. 1996, https://doi.org/10.1007/BF00356014

[4] B. J. Cardwell and A. F. Yee, “Toughening of epoxies through thermoplastic crack bridging,” 1998.

[5] C. Thanomsilp and P. J. Hogg, “Penetration impact resistance of hybrid composites based on commingled yarn fabrics,” *Composites Science and Technology*, vol. 63, no. 3-4, pp. 467–482, Feb 2003, https://doi.org/10.1016/S0266-3538(02)00233-6

[6] P. J. Hogg, “Toughening of thermosetting composites with thermoplastic fibres,” *Materials Science and Engineering: A*, vol. 412, no. 1–2, pp. 97–103, Dec. 2005, https://doi.org/10.1016/j.msea.2005.08.028

[7] M. Hojo, S. Matsuda, M. Tanaka, S. Ochiai, and A. Murakami, “Mode I delamination fatigue properties of interlayer-toughened CF/epoxy laminates,” *Composites Science and Technology*, 2006, https://doi.org/10.1016/j.compscitech.2005.07.038

[8] M. R. Groleau, Y. B. Shi, A. F. Yee, J. L. Bertram, H. J. Sue, and P. C. Yang, “Mode II fracture of composites interlayered with nylon particles,” *Composites Science and Technology*, 1996, https://doi.org/10.1016/S0266-3538(96)00080-2

[9] G. Caprino, P. Iaccarino, and A. Lamboglia, “The effect of shear on the rigidity in three- point bending of unidirectional CFRP laminates made of T800H/3900-2,” *Composite Structures*, 2009, https://doi.org/10.1016/j.compstruct.2008.04.014

[10] T. K. Tsotsis, “Interlayer toughening of composite materials,” *Polymer Composites*, 2009, https://doi.org/10.1002/pc.20535

[11] J. P. Favre, “Improving the fracture energy of carbon fibre-reinforced plastics by delamination promoters,” *Journal of Materials*

Science, 1977, https://doi.org/10.1007/BF00738470

[12] J. E. Masters, "Improved Impact and Delamination Resistance through Interleafing," *Key Engineering Materials*, 1989, https://doi.org/10.4028/www.scientific.net/KEM.37.317

[13] W. J. Cantwell and J. Morton, "Impact perforation of carbon fibre reinforced plastic," *Composites Science and Technology*, vol. 38, no. 2, pp. 119–141, Jan. 1990, https://doi.org/10.1016/0266-3538(90)90002-M

[14] W. J. Cantwell and J. Morton, "Detection of impact damage in CFRP laminates," *Composite Structures*, vol. 3, no. 3–4, pp. 241–257, Jan. 1985, https://doi.org/10.1016/0263- 8223(85)90056-X

[15] E. Sevkat, B. Liaw, F. Delale, and B. B. Raju, "Drop-weight impact of plain-woven hybrid glass-graphite/toughened epoxy composites," *Composites Part A: Applied Science and Manufacturing*, 2009, https://doi.org/10.1016/j.compositesa.2009.04.028

[16] J. Gustin, A. Joneson, M. Mahinfalah, and J. Stone, "Low velocity impact of combination Kevlar/carbon fiber sandwich composites," *Composite Structures*, 2005, https://doi.org/10.1016/j.compstruct.2004.07.020

[17] D. Heflin, J. Dustin, and J.-A. Mansson, "Characterization of Adhesion Between Dissimilar Polymer-Matrix Composites," Apr. 2019. https://doi.org/10.33599/nasampe/s.19.1504

[18] "Standard Test Method for Measuring the Damage Resistance of a Fiber-Reinforced Polymer-Matrix Composite to a Concentrated Quasi-Static Indentation Force 1", https://doi.org/10.1520/D6264_D6264M-17

[19] "Standard Test Method for Measuring the Damage Resistance of a Fiber-Reinforced Polymer Matrix Composite to a Drop-Weight Impact Event 1", https://doi.org/10.1520/D7136_D7136M-20

[20] B. L. Wardle and P. A. Lagace, "On the Use of Dent Depth as an Impact Damage Metric for Thin Composite Structures:," vol. 16, no. 12, pp. 1093–1110, Aug. 2016, https://doi.org/10.1177/073168449701601202

[21] J. A. Nixon, M. G. Phillips, D. R. Moore, and R. S. Prediger, "A study of the development of impact damage in cross-ply carbon fibre/PEEK laminates using acoustic emission," *Composites Science and Technology*, vol. 31, no. 1, pp. 1–14, Jan. 1988, https://doi.org/10.1016/0266-3538(88)90073-5

[22] A. T. Nettles, M. J. Douglas, and E. E. Estes, "Scaling Effects in Carbon/epoxy Laminates Under Transverse Quasi-static Loading - Alan T. Nettles - Google Books," Hampton, Virginia, 1999. Accessed: Mar. 20, 2022.

[23] K. Taki, S. Nakamura, T. Takayama, A. Nemoto, and H. Ito, "Direct joining of a laser- ablated metal surface and polymers by precise injection molding," *Microsystem Technologies*, vol. 22, no. 1, pp. 31–38, Jan. 2016, https://doi.org/10.1007/S00542-015-2640- 2/FIGURES/13

[24] K. Ramani and J. Tagle, "Process-induced effects in thin-film bonding of PEKEKK in metal-polymer joints," *Polymer Composites*, vol. 17, no. 6, pp. 879–886, 1996, https://doi.org/10.1002/PC.10681

[25] K. Ramani and W. Zhao, "The evolution of residual stresses in thermoplastic bonding to metals," *International Journal of Adhesion and Adhesives*, vol. 17, no. 4, pp. 353–357, 1997, https://doi.org/10.1016/S0143-7496(97)00030-4

[26] K. Ramani and B. Moriarty, "Thermoplastic bonding to metals via injection molding for macro-composite manufacture," *Polymer Engineering and Science*, vol. 38, no. 5, pp. 870–877, 1998, https://doi.org/10.1002/PEN.10253

[27] K. Enami, F. Kimura, K. Yokoyama, T. Murakami, and Y. Kajihara, "Experimental and simulative investigation of the effects of laser-structured metal surface on metal-polymer direct joining," *Precision Engineering*, vol. 62, pp. 273–281, Mar. 2020, https://doi.org/10.1016/J.PRECISIONENG.2019.12.011

[28] P. A. Fabrin, M. E. Hoikkanen, and J. E. Vuorinen, "Adhesion of thermoplastic elastomer on surface treated aluminum by injection molding," *Polymer Engineering & Science*, vol. 47, no. 8, pp. 1187–1191, Aug. 2007, https://doi.org/10.1002/PEN.20801